On Misalignment Between Magnetometer and Inertial Sensors

Yuanxin Wu, *Senior Member, IEEE*, and Shitu Luo

***Abstract*— Magnetometer, gyroscope, and accelerometer are commonly used sensors in a variety of applications. In addition to sensor's physical imperfection, magnetometer's parameters are also affected by magnetic disturbance. Specifically, the soft-iron magnetic effect not only changes its intrinsic model parameters, including the scale factor, orthogonality matrix, and bias, but also its relative misalignment with respect to other sensors, such as inertial sensors of interest in this paper. Almost all existing methods rely on the local gravity information for cross-sensor calibration, thus requiring to collect accelerometer measurements at static positions. Based on the rationale that in a homogenous magnetic field the magnetometer's measurement variation is exclusively induced by orientation change, this paper proposes a novel magnetometer-inertial sensor misalignment estimation algorithm requiring no local gravity information. Founded on a constrained optimization, the algorithm is recursive in time with self-initialization and is also capable of estimating the gyroscope bias as an added benefit. Field test results show that the proposed algorithm has quite good estimation accuracy. As it is inherently immune to any acceleration disturbance, the test equipment does not have to keep still for effective measurement.**

***Index Terms*— Magnetometer, gyroscope bias, accelerometer, misalignment, soft-iron magnetic effect.**

I. Introduction

MAGNETOMETER, gyroscope and accelerometer have nowadays become commonly used sensors in a variety of applications including but not limited to pedestrian indoor navigation, flight stabilization, satellite attitude, augmented reality, human body motion tracking and medical instrument. Magnetometer measures the ambient magnetic field; gyroscope and accelerometer respectively sense the angular velocity and non-gravitational acceleration of the rigidly-attached platform. The latter two are collectively known as inertial sensors. With the advancing MEMS technology, these sensors have been integrated into an all-in-one compact and low cost sensor module or chip [1]. Among the three kinds of sensors, magnetometer requires special attention as it is prone to the magnetic disturbance in the surrounding environment, such as the ferromagnetic material and strong electric currents. When the magnetometer is placed rigidly on or near to ferromagnetic objects, its output is distorted and cannot measure the external magnetic field, so careful calibration is necessary each time the magnetometer is used [2]. The distortion can be divided into hard iron and soft iron effects. The hard iron effect is simply the additive magnetic field produced by permanent magnets or electrical currents, while the soft iron effect is induced by materials that generate their own magnetic field in response to and distort the underlying magnetic field in both intensity and orientation. Recent progress shows that MEMS magnetometers could avoid magnetic materials and so the soft iron effect [3], [4], but there are still other magnetic materials to consider, e.g., those of other sensors or the platform. The three-axis magnetometer also exhibits scale factor, cross-coupling and bias errors, but these errors behave in the same manner with and are not discriminable from the soft/hard iron effects [5].

The calibration task involves not only the intrinsic sensor calibration but also the cross-sensor calibration, for instance, the frame misalignment between any two sensors. Both intrinsic and cross-sensor calibrations are equally important to high quality application using fused information from multiple sensors, like magnetometer and inertial sensors of interest herein. Specifically, the calibration parameters of gyroscopes and accelerometers (e.g., the scale factor, non-orthogonality and their misalignment) are relatively fixed, but it is quite another story as far as a magnetometer is concerned due to the presence of its unique soft-iron effect [6]. Classical magnetometer calibration techniques (like the swing method [7]) require levelling and external known heading sources. However, end users prefer to an in-situ calibration with no requirement of external equipment. This practical demand gives birth to a class of attitude-independent calibration methods [2], [8]–[13], first proposed in public literature by [11] and [12] and becoming popular in the last decade. These methods exploit the fact that the magnitude of magnetometer measurement is constant regardless of the orientation at the local position. The idea has also been applied to calibrate an inertial measurement unit (IMU) comprised of the accelerometer triad and the gyroscope triad [10], [13]–[17]. The attitude-independent method solves only the intrinsic sensor calibration and is incapable of the cross-sensor calibration as the magnitude of

Manuscript received March 23, 2016; accepted June 16, 2016. Date of publication June 21, 2016; date of current version July 18, 2016. This work was supported in part by the Fok Ying Tung Foundation under Grant 131061, in part by the Hunan Provincial Natural Science Foundation of China under Grant 2015JJ1021, and in part by the National Natural Science Foundation of China under Grant 61174002 and Grant 61422311. The associate editor coordinating the review of this paper and approving it for publication was Prof. Istvan Barsony. *(Corresponding author: Yuanxin Wu.)*

Y. Wu is with the Shanghai Key Laboratory of Navigation and Location-Based Services, School of Electronic Information and Electrical Engineering, Shanghai Jiao Tong University, Shanghai 200240, China, and also with the School of Aeronautics and Astronautics, Central South University, Changsha 410083, China (e-mail: yuanx_wu@hotmail.com).

S. Luo is with Hunan City-Matrix Technology Company Ltd., Changsha 410073, China (e-mail: luoshitu@163.com).

Digital Object Identifier 10.1109/JSEN.2016.2582751

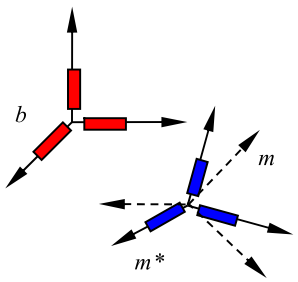

Fig. 1. Gyroscope triad, magnetometer triad and their sensor frames. Filled blocks mean separate sensors. Solid frames (b-frame and m^*-frame) mean senor frames defined by physical sensitivity axes and the dashed frame (m-frame) is the equivalent magnetometer frame induced by soft-iron effect.

the magnetometer measurement is not affected by orientation at all, so a special technique has to be further developed to deal with the cross-sensor misalignment between magnetometer and inertial sensors. The work [18] estimates the mutual misalignment for accelerometer and magnetometer using the invariant angle formed by the local gravity vector and the local magnetic field vector. The method proposed in [10] uses the incremental rotation, calculated by integrating the calibrated gyroscope measurement, as a reference to determine the cross-sensor misalignment of magnetometer relative to gyroscope or between inertial sensors. The works [13], [19] propose to solve the magnetometer calibration by formulating the intrinsic and cross-sensor calibration all together as a maximum likelihood estimation. Almost all methods in previous works, for example [10], [13], [18], [19], rely on the local gravity information for the cross-sensor calibration, thus requiring to collect accelerometer measurements at static positions, and any disturbed acceleration would inevitably decay the cross-sensor calibration quality. As the magnetometer should be calibrated prior to each usage, successively tumbling and keeping still for effective measurements is a very stringent demand for vast applications.

In this regards, this paper investigates a novel cross-sensor calibration approach by only using magnetometer and gyroscope information. It is based on the rationale that in a homogenous magnetic field the magnetometer's measurement variation is exclusively induced by orientation change. The paper is organized as follows. Section II describes sensor models and the misalignment problem of magnetometer and gyroscope. Section III formulates the problem as a constrained minimization and designs a recursive algorithm for joint estimation of the cross-sensor misalignment and the gyroscope bias. Section IV reports the field test result and the conclusions are drawn in Section V.

II. Sensor Model and Misalignment Problem

This paper focuses the cross-sensor calibration problem, and the three-axis magnetometer and the three-axis gyroscope are assumed having been intrinsically calibrated in their separate sensor frames by appropriate attitude-independent methods [2], [8], [10]. Figure 1 illustrates the magnetometer senor frame (m^*-frame) and the gyroscope sensor frame (b-frame), defined by the their sensors' physical sensitivity axes. For example, m^*-frame could be defined as such: z-axis aligned with the z-sensor, y-axis orthogonal to z-axis in the plane formed by z-sensor and y-sensor, and x-axis naturally defined by the right-handed rule. It is common that the two frames misalign each other by m^* some amount of angles. As discussed below, the equivalent m-frame in the presence of soft-iron disturbance may be quite distinctive from the physical m^*-frame. It is an unique characteristic of the magnetometer.

A. Gyroscope and Orientation

The intrinsically calibrated gyroscope measures the platform's angular velocity relative to the inertial space, expressed in the gyroscope frame, namely, $\boldsymbol{\omega}_{ib}^{b}$. The platform orientation with some reference frame, like the Earth frame (e-frame), can be computed by integrating gyroscope measurements [5]

$$\dot{\mathbf{C}}_b^e = \mathbf{C}_b^e \left(\boldsymbol{\omega}_{ib}^b - \boldsymbol{\varepsilon} - \boldsymbol{\omega}_{ie}^b\right)\times \approx \mathbf{C}_b^e \left(\boldsymbol{\omega}_{ib}^b - \boldsymbol{\varepsilon}\right)\times \tag{1}$$

where $\mathbf{C}_b^e$ is the orientation matrix (orthogonal with positive determinant) of e-frame relative to b-frame, $\boldsymbol{\varepsilon}$ denotes the gyroscope bias and $\boldsymbol{\omega}_{ie}^b$ is the Earth's rotation angular velocity relative to the inertial space. The reason the gyroscope bias is considered here is that it is somewhat random at each start-up and thus cannot be calibrated and compensated once for all. The skew symmetric matrix $(\cdot\times)$ is defined so that the cross product satisfies $\mathbf{x}\times\mathbf{y} = (\mathbf{x}\times)\,\mathbf{y}$ for arbitrary two vectors. For applications using low-cost MEMS gyroscopes, the quantity $\boldsymbol{\omega}_{ie}^b$ is rather small in magnitude ($\approx$ 0.004 deg/s) compared with the gyroscope bias $\boldsymbol{\varepsilon}$, so it is reasonable to regard the Earth frame as an inertially-fixed frame for those low-cost applications [10], [13], [14], [17] and the adverse effect of disregarding the Earth rotation is negligible.

No analytical solution to (1) exists except when the angular velocity is invariant in direction. In this special case, the angular velocity is related to the resultant incremental rotation over a short time interval δt as [5], [20]

$$\begin{aligned}\mathbf{C}_{b(t+\delta t)}^{b(t)} &= \mathbf{I} + \frac{\sin\left(\|\boldsymbol{\sigma}\|\right)}{\|\boldsymbol{\sigma}\|}\boldsymbol{\sigma}\times + \frac{1-\cos\left(\|\boldsymbol{\sigma}\|\right)}{\|\boldsymbol{\sigma}\|^2}\left(\boldsymbol{\sigma}\times\right)^2 \\ &\approx \mathbf{I} + \boldsymbol{\sigma}\times\end{aligned} \tag{2}$$

where $\boldsymbol{\sigma} \equiv \delta t\ \left(\boldsymbol{\omega}_{ib}^b - \boldsymbol{\varepsilon}\right)$ and $\|\cdot\|$ denotes the vector magnitude.

B. Magnetometer and Local Magnetic Field

This subsection explains how the soft-iron effect changes the magnetometer frame. Taking the time-invariant magnetic disturbance and sensor imperfection into account, the magnetometer measurement can be collectively modelled by [8], [10]

$$\mathbf{y} = \mathbf{S}\mathbf{C}_e^{m*}\mathbf{m}^e + \mathbf{h} \tag{3}$$

where $\mathbf{C}_e^{m*}$ is the orientation matrix of m*-frame relative to e-frame and $\mathbf{m}^e$ is the typically unknown local magnetic vector in e-frame. For a homogenous magnetic field at the calibration site, $\mathbf{m}^e$ is constant and assumed to have unity norm without loss of generality. The parameters $\mathbf{S}$ and $\mathbf{h}$ encode the compound effect of sensor imperfection and magnetic disturbance. Specifically, $\mathbf{S}$ can be further decomposed as

$\mathbf{S} = \mathbf{\Lambda}_I \mathbf{M}_I \mathbf{S}_M$, where $\mathbf{\Lambda}_I$ is the scale factor diagonal matrix, $\mathbf{M}_I$ is the upper triangular non-orthogonality matrix and $\mathbf{S}_M$ denotes the soft-iron effect matrix [8]. The subscript 'I' means physical imperfection and 'M' means magnetic disturbance. It can be predicted that the right-multiplying soft-iron matrix will distort the above-defined m^*-frame into another equivalent frame (m-frame in Fig. 1). This m-frame distortion effect will be explained later in Section IV. Once the soft-iron disturbance changes, new calibration would have to be performed to find a new equivalent frame. Alternatively, assume $\mathbf{S}^{-1} = \mathbf{QR}$ by the orthogonal-triangular (QR) decomposition, where $\mathbf{Q}$ is orthogonal and $\mathbf{R}$ is upper triangular with positive diagonal entries [2]. The first item on the right of (3)

$$\mathbf{S}\mathbf{C}_e^{m*}\mathbf{m}^e = \mathbf{R}^{-1}\mathbf{Q}^T\mathbf{C}_e^{m*}\mathbf{m}^e \equiv \mathbf{R}^{-1}\mathbf{m}^m \tag{4}$$

Substituting into (3) yields the widely used intrinsic magnetometer calibration model

$$\mathbf{m}^m = \mathbf{R}\left(\mathbf{y} - \mathbf{h}\right),$$

with

$$\left\|\mathbf{m}^m\right\| = \left\|\mathbf{Q}^T\mathbf{C}_e^{m*}\mathbf{m}^e\right\| = 1 \tag{5}$$

The upper triangular matrix $\mathbf{R}$ can be further re-written as a matrix product of $\mathbf{M}^{-1}\mathbf{\Lambda}^{-1}$, where $\mathbf{\Lambda}$ is a diagonal matrix making the diagonal of $\mathbf{M}$ be all ones. We call $\mathbf{\Lambda}$ the equivalent scale factor matrix and $\mathbf{M}$ the equivalent non-orthogonality matrix. It can be deduced from the above discussion that they are both potentially affected by the soft-iron effect.

C. Calibrated Gyroscope/Magnetometer and Their Misalignment

Gyroscope senses angular velocity, magnetometer senses magnetic field, and their measurements are different physical entities in nature. In order to determine their frame misalignment, we must find a way to bridge these two kinds of physical entities. The intrinsically calibrated magnetometer output measures the local magnetic vector by

$$\mathbf{m}^m(t) = \mathbf{C}_b^m\mathbf{C}_e^b(t)\,\mathbf{m}^e \tag{6}$$

in which $\mathbf{C}_b^m$ denotes the frame misalignment of m-frame relative to b-frame and is a constant parameter (for fixed soft-iron disturbance) to be determined by the cross-sensor calibration. Equation (6) shows that in a homogenous magnetic field the magnetometer's measurement ($\mathbf{m}^m$) variation can only be caused by the orientation change of $\mathbf{C}_e^b$. Their time dependences are explicitly stated. Taking time derivative on both sides of (6), and using (1) and the property of an orientation matrix yields

$$\begin{aligned}\dot{\mathbf{m}}^m(t) &= -\mathbf{C}_b^m\left(\left(\boldsymbol{\omega}_{ib}^b(t) - \boldsymbol{\varepsilon}\right)\times\right)\mathbf{C}_e^b(t)\,\mathbf{m}^e \\ &= -\mathbf{C}_b^m\left(\left(\boldsymbol{\omega}_{ib}^b(t) - \boldsymbol{\varepsilon}\right)\times\right)\mathbf{C}_m^b\mathbf{m}^m(t) \\ &= \left(\mathbf{m}^m(t)\times\right)\mathbf{C}_b^m\left(\boldsymbol{\omega}_{ib}^b(t) - \boldsymbol{\varepsilon}\right)\end{aligned} \tag{7}$$

Integrating over the time interval $[t_k \quad t_{k+1}]$,

$$\mathbf{m}^m(t_{k+1}) - \mathbf{m}^m(t_k) = \int_{t_k}^{t_{k+1}}\left(\mathbf{m}^m(t)\times\right)\mathbf{C}_b^m\left(\boldsymbol{\omega}_{ib}^b(t) - \boldsymbol{\varepsilon}\right)dt \tag{8}$$

This exactly relates the magnetometer measurement to the gyroscope measurement by way of the misalignment $\mathbf{C}_b^m$.

Alternatively, for time instants t_k and t_{k+1}, $\mathbf{m}^m(t_k) = \mathbf{C}_b^m\mathbf{C}_e^b(t_k)\,\mathbf{m}^e$ and $\mathbf{m}^m(t_{k+1}) = \mathbf{C}_b^m\mathbf{C}_e^b(t_{k+1})\,\mathbf{m}^e$ according to (6). From the former equation, $\mathbf{m}^e = \mathbf{C}_b^e(t_k)\,\mathbf{C}_m^b\mathbf{m}^m(t_k)$. Substituting into the latter equation and using the inertially-fixed Earth frame assumption again

$$\begin{aligned}\mathbf{m}^m(t_{k+1}) &= \mathbf{C}_b^m\mathbf{C}_e^b(t_{k+1})\,\mathbf{C}_b^e(t_k)\,\mathbf{C}_m^b\mathbf{m}^m(t_k) \\ &\approx \mathbf{C}_b^m\mathbf{C}_{b(t_k)}^{b(t_{k+1})}\mathbf{C}_m^b\mathbf{m}^m(t_k)\end{aligned} \tag{9}$$

It connects the magnetometer measurement with the incremental orientation $\mathbf{C}_{b(t_k)}^{b(t_{k+1})}$ that is further related to the gyroscope measurement through (2). Equation (9) was reportedly used in [10] to estimate the misalignment, but no details have been given on the influence of unknown gyroscope bias, estimation accuracy and how to obtain a good initial value. Using (2), it can be shown that (9) is in fact an approximation of (8) for a small $\delta t \equiv t_{k+1} - t_k$

$$\begin{aligned}\mathbf{C}_b^m\mathbf{C}_{b(t_k)}^{b(t_{k+1})}\mathbf{C}_m^b &\approx \mathbf{C}_b^m\left(\mathbf{I} - \delta t\left(\boldsymbol{\omega}_{ib}^b - \boldsymbol{\varepsilon}\right)\times\right)\mathbf{C}_m^b \\ &= \mathbf{I} - \delta t\left(\mathbf{C}_b^m\left(\boldsymbol{\omega}_{ib}^b - \boldsymbol{\varepsilon}\right)\right)\times\end{aligned} \tag{10}$$

Substituting into (9) yields (8) yet with rectangular approximation to the integral therein. Contrasting (9), it is another notable benefit of (8) that the gyroscope bias appears explicitly therein, which makes possible the estimation of the gyroscope bias.

III. Joint Misalignment and Bias Estimation

This section will formulate a minimization problem to jointly estimate the frame misalignment and the gyroscope bias. Rewrite (8) as

$$\begin{aligned}&\mathbf{m}^m(t_{k+1}) - \mathbf{m}^m(t_k) \\ &= \left[\int_{t_k}^{t_{k+1}}\boldsymbol{\omega}_{ib}^{bT}(t)\otimes\left(\mathbf{m}^m(t)\times\right)dt \quad -\int_{t_k}^{t_{k+1}}\left(\mathbf{m}^m(t)\times\right)dt\right] \\ &\quad\times\begin{bmatrix} vec\left(\mathbf{C}_b^m\right) \\ \mathbf{C}_b^m\boldsymbol{\varepsilon}\end{bmatrix} \equiv \begin{bmatrix}\mathbf{W}_k & \mathbf{M}_k\end{bmatrix}_{3\times 12}\begin{bmatrix} vec\left(\mathbf{C}_b^m\right) \\ \boldsymbol{\varepsilon}_m\end{bmatrix}, \\ &\qquad\qquad k = 0, 1, 2\ldots\end{aligned} \tag{11}$$

where the operator $\otimes$ denotes the Kronecker product and $vec(\mathbf{A})$ forms a vector by stacking the columns of the matrix $\mathbf{A}$. The matrix equality $vec(\mathbf{ABC}) = \left(\mathbf{C}^T\otimes\mathbf{A}\right)vec(\mathbf{B})$ has been used above. Equation (11) is linear in the augmented parameter $\left[vec^T\left(\mathbf{C}_b^m\right)\ \boldsymbol{\varepsilon}_m^T\right]^T$. The SO(3) constraint posed by the orientation matrix $\mathbf{C}_b^m$ should be exploited to achieve an optimal estimate. Suppose the time interval length $t_{k+1} - t_k$ is an integer, say M, times of the sensor sampling interval Δ. The integrals in the subjective can be approximated by the trapezoidal rule using gyroscope/magnetometer

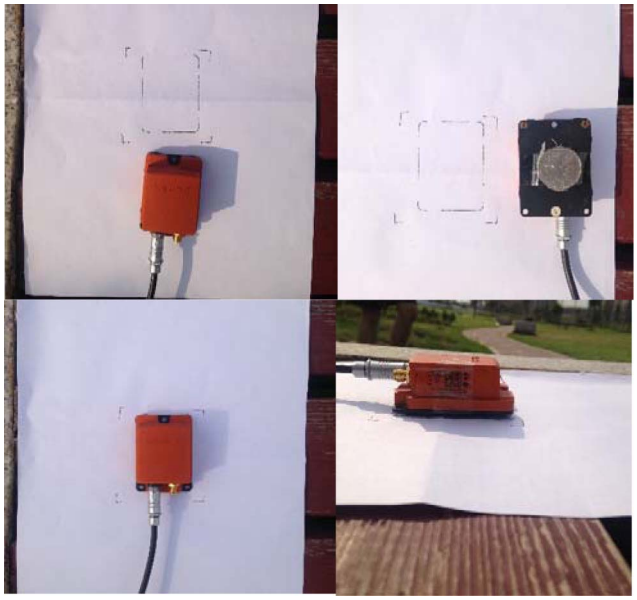

Fig. 2. Test unit (Xsens MTi-G-700) and placement at still as indicated by rectangular (upper-right: a coin attached at unit bottom for Tests #H-I).

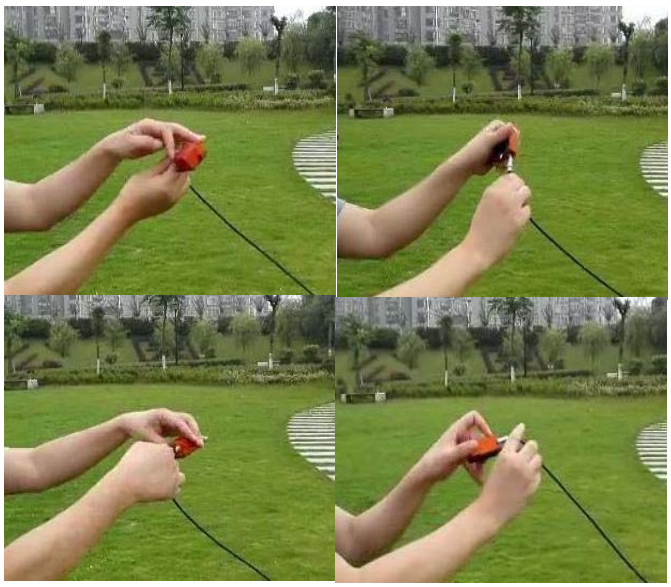

Fig. 3. Tumbling unit by hand for data collecting (screenshots from test video).

measurements

$$\mathbf{W}_k = \sum_{j=0}^{M-1} \int_{t_k+j\Delta}^{t_k+(j+1)\Delta} \boldsymbol{\omega}_{ib}^{bT}(t) \otimes \left(\mathbf{m}^m(t)\times\right) dt$$
$$= \frac{\Delta}{2} \sum_{j=0}^{M-1} \left(\boldsymbol{\omega}_{ib}^{bT}(t) \otimes \left(\mathbf{m}^m(t)\times\right)\Big|_{t_k+j\Delta} + \boldsymbol{\omega}_{ib}^{bT}(t) \otimes \left(\mathbf{m}^m(t)\times\right)\Big|_{t_k+(j+1)\Delta} \right) \quad (12)$$

$$\mathbf{M}_k = -\sum_{j=0}^{M-1} \int_{t_k+j\Delta}^{t_k+(j+1)\Delta} \left(\mathbf{m}^m(t)\times\right) dt$$
$$= -\frac{\Delta}{2} \sum_{j=0}^{M-1} \left(\mathbf{m}^m(t_k+j\Delta)\times + \mathbf{m}^m(t_k+(j+1)\Delta)\times\right) \quad (13)$$

The joint estimation can be written as a problem of minimization

$$\min_{\mathbf{C}\in SO(3),\boldsymbol{\varepsilon}_m} \sum_k \left\| \mathbf{W}_k vec(\mathbf{C}) + \mathbf{M}_k \boldsymbol{\varepsilon}_m - \left(\mathbf{m}^m(t_{k+1}) - \mathbf{m}^m(t_k)\right)\right\|^2$$
$$\equiv \min_{\mathbf{C}\in SO(3),\boldsymbol{\varepsilon}_m} g(\mathbf{C}, \boldsymbol{\varepsilon}_m) \quad (14)$$

or alternatively expressed in unit quaternion as

$$\min_{\mathbf{q}\in S^3,\boldsymbol{\varepsilon}_m} \sum_k \left\| \mathbf{W}_k vec(\mathbf{C}(\mathbf{q})) + \mathbf{M}_k \boldsymbol{\varepsilon}_m - \left(\mathbf{m}^m(t_{k+1}) - \mathbf{m}^m(t_k)\right)\right\|^2$$
$$\equiv \min_{\mathbf{q}\in S^3,\boldsymbol{\varepsilon}_m} f(\mathbf{q}, \boldsymbol{\varepsilon}_m) \quad (15)$$

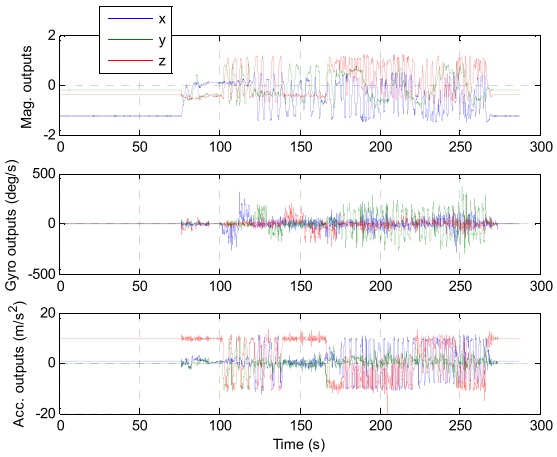

Fig. 4. Magnetometer, gyroscope and accelerometer outputs in Test #1 (unit status sequence: still at placement, picked up, short still, tumbling, short still, put back, still at same placement).

where S^3 denotes the set of 4-by-1 unit vectors and the quaternion ($\mathbf{q} \equiv [q_0\ q_1\ q_2\ q_3]^T$) is related to the orientation matrix by [5], [21], (16), as shown at the bottom of this page.

The above problem is a constrained least square that could be well solved by the efficient Newton method [22], given a good initial guess of the orientation matrix in (14) or the orientation quaternion in (15). The formulation (15) is more preferable as it is conditioned on a four-element quaternion instead of a nine-element matrix.

$$\mathbf{C}(\mathbf{q}) = \begin{bmatrix} q_0^2+q_1^2-q_2^2-q_3^2 & 2(q_1q_2+q_0q_3) & 2(q_1q_3-q_0q_2) \\ 2(q_1q_2-q_0q_3) & q_0^2-q_1^2+q_2^2-q_3^2 & 2(q_2q_3+q_0q_1) \\ 2(q_1q_3+q_0q_2) & 2(q_2q_3-q_0q_1) & q_0^2-q_1^2-q_2^2+q_3^2 \end{bmatrix} \quad (16)$$

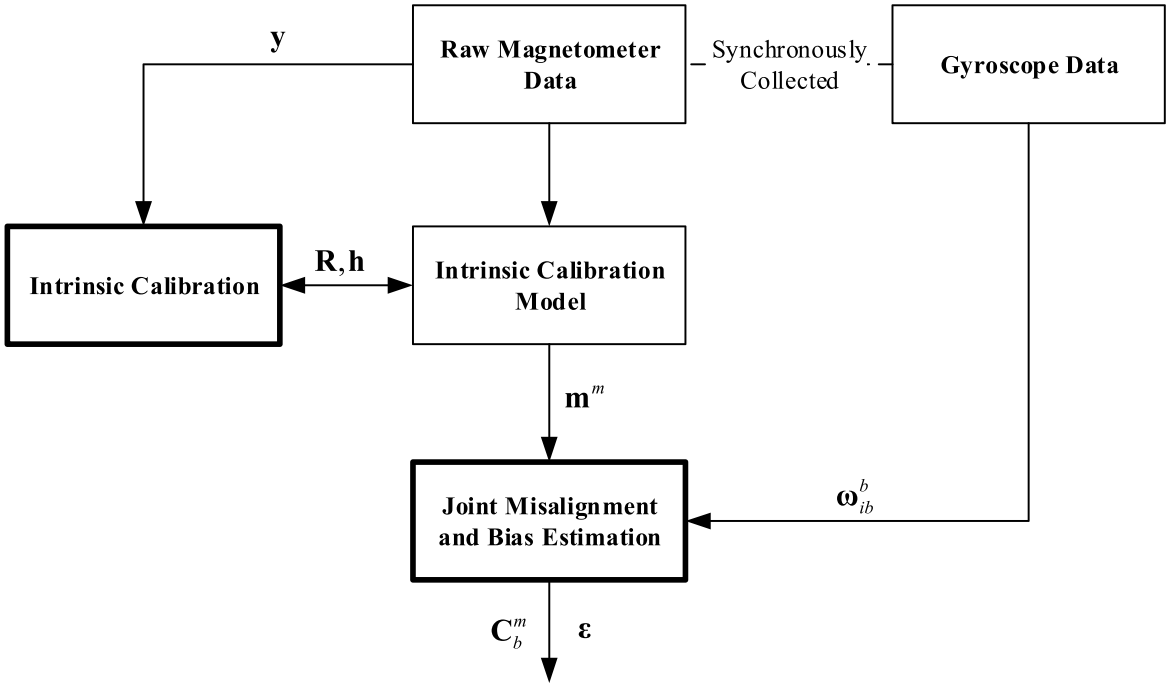

Fig. 5. Flowchart for intrinsic calibration, cross-sensor calibration and gyroscope bias estimation.

A. Batch Algorithm

Specifically, the Newton method updates the estimate as such

$$\mathbf{x}^{(i+1)} = \mathbf{x}^{(i)} - \left[\nabla_{\mathbf{x}}^2 J\Big|_{\mathbf{x}^{(i)}}\right]^{-1}\left(\nabla_{\mathbf{x}} J|_{\mathbf{x}^{(i)}}\right), \quad i = 0, 1, \ldots \tag{17}$$

where $\nabla_{\mathbf{x}} J$ is the Jacobian vector and $\nabla_{\mathbf{x}}^2 J$ is the Hessian matrix of the objective with respect to the estimate $\mathbf{x}$. For the current minimization problem, the estimate $\mathbf{x} = [\mathbf{q}^T \ \boldsymbol{\varepsilon}_m^T \ \lambda]^T$ and the subjective $J(\mathbf{x}) = f(\mathbf{q}, \boldsymbol{\varepsilon}_m) + \lambda(\mathbf{q}^T\mathbf{q} - 1)$, where λ is the Lagrange coefficient for the unity norm constraint of the orientation quaternion. The Jacobian vector and Hessian matrix are given in Appendix A for brevity.

A fine initial orientation quaternion for (17) can be derived by relaxing the constraint in (14), namely, regarding the orientation matrix $\mathbf{C}_b^m$ therein as a common matrix. Then the unconstrained minimization (14) is simplified to a common linear least-square problem that yields

$$\begin{bmatrix} vec\left(\mathbf{C}_b^m\right) \\ \boldsymbol{\varepsilon}_m \end{bmatrix} = \left(\sum_k \begin{bmatrix} \mathbf{W}_k & \mathbf{M}_k \end{bmatrix}^T \begin{bmatrix} \mathbf{W}_k & \mathbf{M}_k \end{bmatrix}\right)^{-1} \times \sum_k \begin{bmatrix} \mathbf{W}_k & \mathbf{M}_k \end{bmatrix}^T \left(\mathbf{m}^m(t_{k+1}) - \mathbf{m}^m(t_k)\right) \tag{18}$$

which generates an initial orientation matrix $\mathbf{C}_b^{m(0)}$ and an initial gyroscope bias $\boldsymbol{\varepsilon}_m^{(0)}$, and after a necessary orthogonalization process, an initial quaternion $\mathbf{q}^{(0)}$ is obtained by (16). The Lagrange coefficient $\lambda^{(0)}$ is set to zero.

B. Recursive Algorithm

The structure of the above algorithm allows for a recursive form in time, which is preferable to many on-line applications. Following the technique proposed in the work [23], we can re-express the entities of the Jacobian vector and Hessian matrix in a recursive way, namely, to take the estimation parameters out of the summation. For the sake of brevity, the development and the resultant recursive algorithm is presented in Appendix B.

IV. Test Results

This section is devoted to verifying the above analysis and algorithm by field tests. Four test datasets were collected using the Xsens MTi-G-700 unit. Each test starts and ends at still, with the unit being placed at an exactly same location on a bench, as shown by the rectangular in Fig. 2. Two datasets (#1 and #2) were collected using the MTi-G-700 unit alone, while the other two (#3 and #4) were collected by taping a RMB ¥1 coin onto the unit bottom plate. The coin is made of soft magnetic material, with steel core and nickel plating (Fig. 2, upper-right). The magnetometer and gyroscope outputs are both sampled at 100Hz, namely, the sampling interval $\Delta = 0.01s$. The time interval length is uniformly set to $t_{k+1} - t_k = 0.5s$ in this section.

The magnetometer, gyroscope and accelerometer outputs in Test #1 are plotted in Fig. 4 as an example. In this test, the unit first stays still on a bench for about 75 seconds, and is then picked up and taken several meters away from the data-collecting desktop. After keeping roughly still in hand for a moment, the unit starts to be continuously tumbled by hand (See screenshots in Fig. 3 taken from test video) for about 170 seconds. Translation motion is restrained as much as possible while tumbling so as to place the unit in a fairly homogeneous magnetic field. Then the test is ended by keeping the unit roughly still for a moment again and putting it back to the placement on the bench. Other datasets follow the same

TABLE I
MISALIGNMENT ESTIMATION TEST RESULTS AND CALIBRATED MAGNETIC FIELD MEASUREMENTS

	Intrinsic Calibration $(\mathbf{R},\mathbf{h})$	Cross-sensor Calibration (deg) $qua2eul\left(\mathbf{q}_b^m\right)$	Calibrated Magnetic Field Measurements at Placement	
Test #1	$\begin{bmatrix} 1.0012 & -0.0032 & 0.0018 \\ 0 & 0.9970 & 0.0015 \\ 0 & 0 & 1.0047 \end{bmatrix}$ $\begin{bmatrix} -0.5001 & 0.0412 & 0.2384 \end{bmatrix}^T$	$\begin{bmatrix} 0.029 & -0.053 & -0.078 \end{bmatrix}^T$	Start:	$\begin{bmatrix} -0.740 & -0.248 & -0.623 \end{bmatrix}^T$
			End:	$\begin{bmatrix} -0.741 & -0.240 & -0.628 \end{bmatrix}^T$
Test #2	$\begin{bmatrix} 1.0012 & -0.0070 & 0.0018 \\ 0 & 0.9973 & 0.0012 \\ 0 & 0 & 1.0045 \end{bmatrix}$ $\begin{bmatrix} -0.4998 & 0.0418 & 0.2382 \end{bmatrix}^T$	$\begin{bmatrix} -0.070 & -0.022 & -0.102 \end{bmatrix}^T$	Start:	$\begin{bmatrix} -0.740 & -0.246 & -0.622 \end{bmatrix}^T$
			End:	$\begin{bmatrix} -0.737 & -0.255 & -0.623 \end{bmatrix}^T$
Test #3	$\begin{bmatrix} 1.2631 & 0.3138 & -0.4183 \\ 0 & 1.5192 & 0.3418 \\ 0 & 0 & 0.8215 \end{bmatrix}$ $\begin{bmatrix} -0.6292 & -0.1036 & -0.2519 \end{bmatrix}^T$	$\begin{bmatrix} 16.255 & 24.097 & 9.983 \end{bmatrix}^T$	Start:	$\begin{bmatrix} -0.449 & -0.409 & -0.804 \end{bmatrix}^T$
			End:	$\begin{bmatrix} -0.432 & -0.408 & -0.803 \end{bmatrix}^T$
			Corrected End:	$\begin{bmatrix} -0.723 & -0.239 & -0.646 \end{bmatrix}^T$
Test #4	$\begin{bmatrix} 1.2631 & 0.3160 & -0.4172 \\ 0 & 1.5160 & 0.3406 \\ 0 & 0 & 0.8236 \end{bmatrix}$ $\begin{bmatrix} -0.6318 & -0.1039 & -0.2474 \end{bmatrix}^T$	$\begin{bmatrix} 16.360 & 23.711 & 10.139 \end{bmatrix}^T$	Start:	$\begin{bmatrix} -0.442 & -0.400 & -0.798 \end{bmatrix}^T$
			End:	$\begin{bmatrix} -0.451 & -0.411 & -0.793 \end{bmatrix}^T$
			Corrected End:	$\begin{bmatrix} -0.731 & -0.249 & -0.636 \end{bmatrix}^T$

motion sequence. Note that the proposed algorithm does not need accelerometer information for estimation and plotting it in Fig. 4 is just for a complete sense of tumbling motion in tests. Acceleration disturbance is not a problem at all here, but would be a big trouble for those methods relying on the local gravity information, as discussed in Section I. The still data before moving is averaged to approximately calculate the gyroscope bias, and the data while the unit being tumbled by hand is used for joint estimation.

The flowchart for the intrinsic calibration and the joint misalignment and gyroscope bias estimation is given in Fig. 5. The magnetometer data collected during tumbling motion (extracted using the two short roughly still time periods) is first used to carry out intrinsic calibration [2] yielding $\mathbf{m}^m$. Then the calibrated magnetometer measurement is processed by the proposed recursive algorithm, together with the collected gyroscope data $\boldsymbol{\omega}_{ib}^b$, to jointly estimate the magnetometer-gyroscope misalignment $\mathbf{C}_b^m$ and the gyroscope bias $\boldsymbol{\varepsilon}$. Figures 6-9 respectively present the joint estimation results for the four datasets, as well as the initial values computed by (18). No results are displayed for the first ten seconds as the data during this period has been accumulated for a better

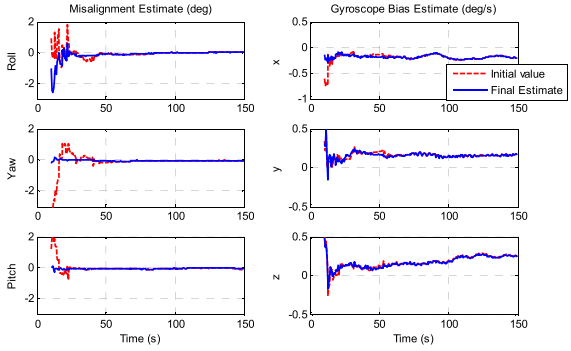

Fig. 6. Misalignment and gyroscope bias estimate for Test #1. (Initial value: red dashed line; Final estimate: blue solid line).

initial value. The initial value given by (18) begins to agree quite well with the recursive algorithm's final estimate after 60s for each dataset. The final misalignment estimates are listed in Table I and the final gyroscope bias estimates are listed in Table II.

As there is no ground truth for misalignment in our tests, the calibrated magnetometer measurements at the placement

TABLE II
GYROSCOPE BIAS ESTIMATES (UNIT: deg/s)

	By Still Averaging	By Algorithm	By Algorithm (Fake Bias Added)
Test #1	$[-0.195 \quad 0.168 \quad 0.256]^T$	$[-0.204 \quad 0.160 \quad 0.243]^T$	$[1.796 \quad 5.160 \quad 3.243]^T$
Test #2	$[-0.252 \quad 0.152 \quad 0.251]^T$	$[-0.198 \quad 0.138 \quad 0.230]^T$	$[1.806 \quad 5.135 \quad 3.228]^T$
Test #3	$[-0.228 \quad 0.147 \quad 0.246]^T$	$[-0.239 \quad 0.062 \quad 0.142]^T$	$[1.760 \quad 5.063 \quad 3.145]^T$
Test #4	$[-0.237 \quad 0.153 \quad 0.250]^T$	$[-0.164 \quad 0.084 \quad 0.173]^T$	$[1.838 \quad 5.082 \quad 3.170]^T$

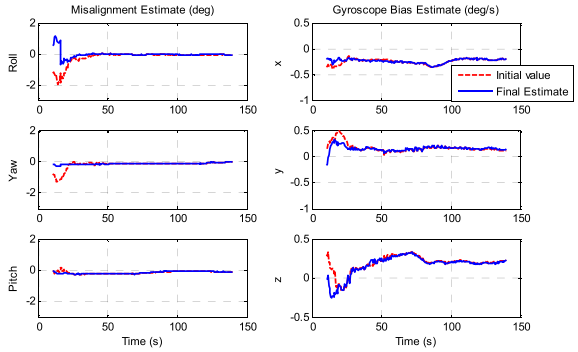

Fig. 7. Misalignment and gyroscope bias estimate for Test #2. (Initial value: red dashed line; Final estimate: blue solid line).

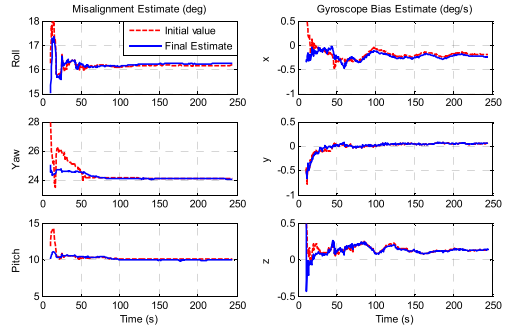

Fig. 8. Misalignment and gyroscope bias estimate for Test #3. (Initial value: red dashed line; Final estimate: blue solid line).

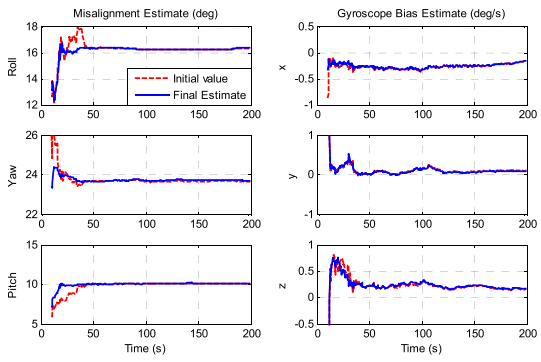

Fig. 9. Misalignment and gyroscope bias estimate for Test #4. (Initial value: red dashed line; Final estimate: blue solid line).

will be used for consistency verification. Table I lists the test results for four datasets of intrinsic calibration and cross-sensor misalignment calibration. We see that the intrinsic parameters are quite consistent between Test #1 and Test #2 and between Test #3 and Test #4, so are the cross-sensor misalignment estimation. However, a significant discrepancy exists between the first two datasets (Tests #1 and #2) and the second two datasets (Tests #3 and #4). The misalignment angle between the magnetometer frame and the gyroscope frame is less than 0.1 degrees before the coin is attached, but increases to as large as 25 degrees after the coin is attached. This hints that the soft-magnetic coin has remarkably changed the relative orientation of the magnetometer frame and the gyroscope frame. As the gyroscope frame is nearly magnetic-proof, that is to say, it is the magnetometer frame that has been changed. Taking Test #1 and Test #4 as an example and decomposing the intrinsic parameter R,

$$R_{\#1} = \begin{bmatrix} 1 & -0.0032 & 0.0018 \\ 0 & 1 & 0.0015 \\ 0 & 0 & 1 \end{bmatrix} \begin{bmatrix} 1.0012 & 0 & 0 \\ 0 & 0.9970 & 0 \\ 0 & 0 & 1.0047 \end{bmatrix}$$
$$R_{\#4} = \begin{bmatrix} 1 & 0.2084 & -0.5066 \\ 0 & 1 & 0.4136 \\ 0 & 0 & 1 \end{bmatrix} \begin{bmatrix} 1.2631 & 0 & 0 \\ 0 & 1.5160 & 0 \\ 0 & 0 & 0.8236 \end{bmatrix} \quad (19)$$

from which the angles between the magnetic sensor axes can be derived: $[90.18 \ 89.90 \ 89.91]^T$ degrees for Test #1 and $[77.97 \ 120.43 \ 65.57]^T$ degrees for Test #4. As discussed in the text below (5), the equivalent scale factor matrix and non-orthogonality matrix are both significantly affected by the soft-magnetic coin.

The last column of Table I gives the intrinsically calibrated magnetic field measurement at the placement at the beginning and ending of each dataset, using the model (5) along with the intrinsic parameters in the 2nd column. These intrinsically calibrated measurements are actually the local magnetic vector expressed in the magnetometer frame (m-frame). As the magnetometer frame has been considerably altered due to the coin attachment, the intrinsically calibrated measurements in Tests #3 and #4 are quite different from those in Tests #1 and #2. Notably, after being corrected by the frame misalignment estimation (3rd column) for Tests #3 and #4 using (6), i.e., $\left(\mathbf{C}_b^m\right)^T \mathbf{m}^m(t)$, all measurements become consistent. In other words, the local magnetic measurements are now expressed in the gyroscope frame that is fixed relative to the

TABLE III
MISALIGNMENT ESTIMATION RESULTS AFTER INTENTIONAL ROTATION (UNIT: DEGREE)

	Original Cross-sensor Misalignment $dcm2eul\left(\mathbf{C}_b^m\right)$	Renewed Cross-sensor Misalignment $dcm2eul\left(\mathbf{C}_m^{\tilde{m}}\mathbf{C}_b^m\right)$	Cross-sensor Calibration
Test #4	$\begin{bmatrix}16.360 & 23.711 & 10.139\end{bmatrix}^T$	$\begin{bmatrix}23.338 & 40.035 & 29.726\end{bmatrix}^T$	$\begin{bmatrix}23.338 & 40.035 & 29.726\end{bmatrix}^T$

Earth at the same placement, so they are supposed to produce roughly the same.

To examine the proposed algorithm's capability, we intentionally rotate the intrinsically calibrated measurements by $\mathbf{C}_m^{\tilde{m}} \equiv eul2dcm\left(\begin{bmatrix}10 & 20 & 15\end{bmatrix}\ \text{deg}\right)$ and evaluate the algorithm using dataset #4. Note that the renewed misalignment now becomes $\mathbf{C}_m^{\tilde{m}}\mathbf{C}_b^m$. As shown in Table III, the proposed algorithm almost perfectly recovers the renewed misalignment result. Table II compares the gyroscope bias estimates by still averaging and those by the algorithm. Among the four datasets, the gyroscope estimate discrepancy is no more than 0.1 deg/s (in Test #3). An additional fake gyroscope bias [2 5 3] (unit: deg/s) is added to the gyroscope measurement $\boldsymbol{\omega}_{ib}^b$ to further investigate the algorithm's capability in estimating gyroscope bias, as listed in the last column of Table II. We see that the estimate difference between the last two columns are almost equal to the added fake gyroscope bias up to 0.005 deg/s.

Our observations clearly indicate that the cross-sensor misalignment calibration is not an optional but an indispensable procedure to obtain accurate measurements. Otherwise, any deduction from the intrinsically-only-calibrated magnetic measurement would be misleading. Finally, we check how the Apple iPhone 5c's Compass application behave by following a similar procedure with the above tests in Fig. 2. The coin is attached to the backside of the iPhone where the readings are mostly affected. The calibration step has been done individually before and after the coin attachment, as instructed by the Compass application (rolling a red ball around a circle by tilting and rotating). A heading discrepancy of 17 degrees is observed, which indicates that the Apple iPhone does not consider the cross-sensor misalignment calibration for its embedded magnetometer.

V. CONCLUSIONS

Magnetometer has to be calibrated prior to each usage, as magnetic disturbance, especially the soft-iron effect, changes its intrinsic model parameters including the scale factors, orthogonality matrix and bias. As a result, its relative misalignment with respect to other sensors, like inertial sensors of interest in this paper, has also been altered. Therefore, the magnetometer calibration task has to consider not only the intrinsic calibration by the popular attitude-independent methods, expressing the local magnetic field vector in the equivalent magnetometer frame that is distinctive from the physical magnetic sensor frame, but also the cross-sensor misalignment calibration that relates the intrinsically-calibrated magnetometer measurement to some reference frame with physical meanings. Based on the rationale that in a homogenous magnetic field the magnetometer's measurement variation is exclusively induced by orientation change, this paper proposes a novel magnetometer-gyroscope misalignment estimation algorithm that is formulated as an unit-quaternion-constrained minimization problem. The proposed algorithm is recursive in time with self-initialization and is capable of estimating the gyroscope bias as well. Comprehensive field tests have been performed and the results show that the proposed algorithm has quite good estimation accuracy. Because the novel algorithm is able to align the magnetometer to the inertial sensors without using local gravity information, it does not require the test equipment to keep still for effective measurement and is actually immune to large acceleration disturbance.

APPENDIX

A. Jacobian Vector and Hessian Matrix in (17)

They can be respectively derived as

$$\nabla_{\mathbf{x}} J = \begin{bmatrix}\mathbf{J}_q^T & \mathbf{J}_{\varepsilon_m}^T & J_\lambda\end{bmatrix}^T \tag{20}$$

$$\nabla_{\mathbf{x}}^2 J = \begin{bmatrix}\mathbf{H}_{qq} & \mathbf{H}_{q\varepsilon_m} & \mathbf{H}_{q\lambda} \\ \mathbf{H}_{q\varepsilon_m}^T & \mathbf{H}_{\varepsilon_m\varepsilon_m} & \mathbf{0}_{3\times 1} \\ \mathbf{H}_{q\lambda}^T & \mathbf{0}_{3\times 1}^T & 0\end{bmatrix} \tag{21}$$

where

$$\begin{aligned}
\mathbf{J}_q &= 2\lambda\mathbf{q} + 2\sum_k \partial_q^T \left(vec\left(\mathbf{C}\left(\mathbf{q}\right)\right)\right)\mathbf{W}_k^T\boldsymbol{\alpha}_k, \\
\mathbf{J}_{\varepsilon_m} &= 2\sum_k \mathbf{M}_k^T\boldsymbol{\alpha}_k, \quad J_\lambda = \mathbf{q}^T\mathbf{q} - 1, \\
\mathbf{H}_{qq} &= 2\lambda\mathbf{I}_4 + 2\sum_k \Big\{\partial_q^T \left(vec(\mathbf{C}(\mathbf{q}))\right)\mathbf{W}_k^T\mathbf{W}_k\partial_q \left(vec(\mathbf{C}(\mathbf{q}))\right) \\
&\qquad + \begin{bmatrix}\mathbf{Q}_0^T\mathbf{W}_k^T\boldsymbol{\alpha}_k & \mathbf{Q}_1^T\mathbf{W}_k^T\boldsymbol{\alpha}_k & \mathbf{Q}_2^T\mathbf{W}_k^T\boldsymbol{\alpha}_k & \mathbf{Q}_3^T\mathbf{W}_k^T\boldsymbol{\alpha}_k\end{bmatrix}^T\Big\}, \\
\mathbf{H}_{q\varepsilon_m} &= 2\sum_k \partial_q^T \left(vec\left(\mathbf{C}\left(\mathbf{q}\right)\right)\right)\mathbf{W}_k^T\mathbf{M}_k, \\
\mathbf{H}_{q\lambda} &= 2\mathbf{q}, \quad \mathbf{H}_{\varepsilon_m\varepsilon_m} = 2\sum_k^{\mathbf{M}_k^T\mathbf{M}_k}
\end{aligned} \tag{22}$$

and

$$\boldsymbol{\alpha}_k \equiv \mathbf{W}_k vec\left(\mathbf{C}\left(\mathbf{q}\right)\right) + \mathbf{M}_k\boldsymbol{\varepsilon}_m - \left(\mathbf{m}^m\left(t_{k+1}\right) - \mathbf{m}^m\left(t_k\right)\right) \tag{23}$$

$$\partial_q\left(vec\left(\mathbf{C}\left(\mathbf{q}\right)\right)\right)=2\begin{bmatrix} q_0 & q_1 & -q_2 & -q_3\\ -q_3 & q_2 & q_1 & -q_0\\ q_2 & q_3 & q_0 & q_1\\ q_3 & q_2 & q_1 & q_0\\ q_0 & -q_1 & q_2 & -q_3\\ -q_1 & -q_0 & q_3 & q_2\\ -q_2 & q_3 & -q_0 & q_1\\ q_1 & q_0 & q_3 & q_2\\ q_0 & -q_1 & -q_2 & q_3 \end{bmatrix} \tag{24}$$

$$\mathbf{Q}_0=\begin{bmatrix} 1 & 0 & 0 & 0\\ 0 & 0 & 0 & -1\\ 0 & 0 & 1 & 0\\ 0 & 0 & 0 & 1\\ 1 & 0 & 0 & 0\\ 0 & -1 & 0 & 0\\ 0 & 0 & -1 & 0\\ 0 & 1 & 0 & 0\\ 1 & 0 & 0 & 0 \end{bmatrix},\quad \mathbf{Q}_1=\begin{bmatrix} 0 & 1 & 0 & 0\\ 0 & 0 & 1 & 0\\ 0 & 0 & 0 & 1\\ 0 & 0 & 1 & 0\\ 0 & -1 & 0 & 0\\ -1 & 0 & 0 & 0\\ 0 & 0 & 0 & 1\\ 1 & 0 & 0 & 0\\ 0 & -1 & 0 & 0 \end{bmatrix},$$

$$\mathbf{Q}_2=\begin{bmatrix} 0 & 0 & -1 & 0\\ 0 & 1 & 0 & 0\\ 1 & 0 & 0 & 0\\ 0 & 1 & 0 & 0\\ 0 & 0 & 1 & 0\\ 0 & 0 & 0 & 1\\ -1 & 0 & 0 & 0\\ 0 & 0 & 0 & 1\\ 0 & 0 & -1 & 0 \end{bmatrix},\quad \mathbf{Q}_3=\begin{bmatrix} 0 & 0 & 0 & -1\\ -1 & 0 & 0 & 0\\ 0 & 1 & 0 & 0\\ 1 & 0 & 0 & 0\\ 0 & 0 & 0 & -1\\ 0 & 0 & 1 & 0\\ 0 & 1 & 0 & 0\\ 0 & 0 & 1 & 0\\ 0 & 0 & 0 & 1 \end{bmatrix} \tag{25}$$

B. Recursive Algorithm for Joint Misalignment and Gyroscope Bias Estimation

The quantity $\boldsymbol{\alpha}_k$ in (23) is re-written as

$$\begin{aligned}\boldsymbol{\alpha}_k &= \begin{bmatrix}\mathbf{W}_k & \mathbf{M}_k & -\left(\mathbf{m}^m\left(t_{k+1}\right)-\mathbf{m}^m\left(t_k\right)\right)\end{bmatrix}\begin{bmatrix} vec\left(\mathbf{C}\left(\mathbf{q}\right)\right)\\ \boldsymbol{\varepsilon}_m\\ 1\end{bmatrix}\\ &\equiv \boldsymbol{\Gamma}_k\mathbf{x}_u\end{aligned} \tag{26}$$

Then we get

$$\mathbf{J}_q = 2\lambda\mathbf{q}+2\partial_q^T\left(vec\left(\mathbf{C}\left(\mathbf{q}\right)\right)\right)\left(\sum_k\mathbf{W}_k^T\boldsymbol{\Gamma}_k\right)\mathbf{x}_u \tag{27}$$

$$\mathbf{J}_{\varepsilon_m} = 2\left(\sum_k\mathbf{M}_k^T\boldsymbol{\Gamma}_k\right)\mathbf{x}_u \tag{28}$$

$$\begin{aligned}\mathbf{H}_{qq} &= 2\lambda\mathbf{I}_4+2\partial_q^T\left(vec\left(\mathbf{C}\left(\mathbf{q}\right)\right)\right)\\ &\quad\times\left(\sum_k\mathbf{W}_k^T\mathbf{W}_k\right)\partial_q\left(vec\left(\mathbf{C}\left(\mathbf{q}\right)\right)\right)\\ &\quad+2\left[\mathbf{Q}_0^T\left(\sum_k\mathbf{W}_k^T\boldsymbol{\Gamma}_k\right)\mathbf{x}_u\quad\mathbf{Q}_1^T\left(\sum_k\mathbf{W}_k^T\boldsymbol{\Gamma}_k\right)\mathbf{x}_u\right.\\ &\qquad\left.\mathbf{Q}_2^T\left(\sum_k\mathbf{W}_k^T\boldsymbol{\Gamma}_k\right)\mathbf{x}_u\quad\mathbf{Q}_3^T\left(\sum_k\mathbf{W}_k^T\boldsymbol{\Gamma}_k\right)\mathbf{x}_u\right]^T\end{aligned} \tag{29}$$

$$\mathbf{H}_{q\varepsilon_m} = 2\partial_q^T\left(vec\left(\mathbf{C}\left(\mathbf{q}\right)\right)\right)\sum_k\mathbf{W}_k^T\mathbf{M}_k, \tag{30}$$

$$\mathbf{H}_{\varepsilon_m\varepsilon_m} = 2\sum_k\mathbf{M}_k^T\mathbf{M}_k \tag{31}$$

Algorithm 1. Recursive Algorithm for Joint Misalignment and Gyroscope Bias Estimation

Denote six incremental quantities (IQ):

$$\begin{aligned}\boldsymbol{\Omega}_k &\equiv \sum_k\mathbf{W}_k^T\mathbf{M}_k,\quad \boldsymbol{\Xi}_k\equiv\sum_k\mathbf{W}_k^T\mathbf{W}_k,\\ \boldsymbol{\Psi}_k &\equiv \sum_k\mathbf{M}_k^T\mathbf{W}_k,\quad \boldsymbol{\Pi}_k\equiv\sum_k\mathbf{M}_k^T\mathbf{M}_k,\\ \boldsymbol{\Lambda}_k &\equiv \sum_k\mathbf{M}_k^T\left(\mathbf{m}^m\left(t_{k+1}\right)-\mathbf{m}^m\left(t_k\right)\right),\\ \boldsymbol{\Theta}_k &\equiv \sum_k\mathbf{W}_k^T\left(\mathbf{m}^m\left(t_{k+1}\right)-\mathbf{m}^m\left(t_k\right)\right)\end{aligned}$$

Step 1: Set $k=0$. Initialize all six IQs to zero.

Step 2: For current k, compute $\mathbf{W}_k$ and $\mathbf{M}_k$ by (12) and (13), and recursively compute the six IQs as

$$\begin{aligned}\boldsymbol{\Omega}_k &= \boldsymbol{\Omega}_{k-1}+\mathbf{W}_k^T\mathbf{M}_k,\\ \boldsymbol{\Xi}_k &= \boldsymbol{\Xi}_{k-1}+\mathbf{W}_k^T\mathbf{W}_k,\\ \boldsymbol{\Psi}_k &= \boldsymbol{\Psi}_{k-1}+\mathbf{M}_k^T\mathbf{W}_k=\boldsymbol{\Omega}_k^T,\\ \boldsymbol{\Pi}_k &= \boldsymbol{\Pi}_{k-1}+\mathbf{M}_k^T\mathbf{M}_k,\\ \boldsymbol{\Lambda}_k &= \boldsymbol{\Lambda}_{k-1}+\mathbf{M}_k^T\left(\mathbf{m}^m\left(t_{k+1}\right)-\mathbf{m}^m\left(t_k\right)\right),\\ \boldsymbol{\Theta}_k &= \boldsymbol{\Theta}_{k-1}+\mathbf{W}_k^T\left(\mathbf{m}^m\left(t_{k+1}\right)-\mathbf{m}^m\left(t_k\right)\right),\end{aligned}$$

then

$$\boldsymbol{\Delta}_k\equiv\sum_k\mathbf{W}_k^T\boldsymbol{\Gamma}_k=\begin{bmatrix}\boldsymbol{\Xi}_k & \boldsymbol{\Omega}_k & -\boldsymbol{\Theta}_k\end{bmatrix}$$

and

$$\boldsymbol{\Phi}_k\equiv\sum_k\mathbf{M}_k^T\boldsymbol{\Gamma}_k=\begin{bmatrix}\boldsymbol{\Psi}_k & \boldsymbol{\Pi}_k & -\boldsymbol{\Lambda}_k\end{bmatrix}$$

from (26).

Step 3: Set $i=0$ and the initial estimate $\mathbf{x}^{(0)}$. The initial frame misalignment is given by (18), i.e., $\begin{bmatrix} vec\left(\mathbf{C}_b^m\right)\\ \boldsymbol{\varepsilon}_m\end{bmatrix}=\boldsymbol{\Xi}_k^{-1}\boldsymbol{\Theta}_k$, from which $\mathbf{q}^{(0)}$ can be obtained.

Step 4: Compute the Jacobian vector and Hessian matrix entities at current estimate $\mathbf{x}^{(i)}$ using (27)-(30) as

$$\begin{aligned}\mathbf{J}_q &= 2\lambda\mathbf{q}^{(i)}+2\partial_q^T\left(vec\left(\mathbf{C}\left(\mathbf{q}^{(i)}\right)\right)\right)\boldsymbol{\Delta}_k\mathbf{x}_u^{(i)},\\ \mathbf{J}_{\varepsilon_m} &= 2\boldsymbol{\Phi}_k\mathbf{x}_u^{(i)},\quad J_\lambda=\mathbf{q}^{(i)T}\mathbf{q}^{(i)}-1,\\ \mathbf{H}_{qq} &= 2\lambda\mathbf{I}_4+2\partial_q^T\left(vec\left(\mathbf{C}\left(\mathbf{q}^{(i)}\right)\right)\right)\boldsymbol{\Xi}_k\partial_q\\ &\quad\times\left(vec\left(\mathbf{C}\left(\mathbf{q}^{(i)}\right)\right)\right)\\ &\quad+2\left[\mathbf{Q}_0^T\boldsymbol{\Delta}_k\mathbf{x}_u^{(i)}\quad\mathbf{Q}_1^T\boldsymbol{\Delta}_k\mathbf{x}_u^{(i)}\quad\mathbf{Q}_2^T\boldsymbol{\Delta}_k\mathbf{x}_u^{(i)}\right.\\ &\qquad\left.\mathbf{Q}_3^T\boldsymbol{\Delta}_k\mathbf{x}_u^{(i)}\right]^T,\\ \mathbf{H}_{q\varepsilon_m} &= 2\partial_q^T\left(vec\left(\mathbf{C}\left(\mathbf{q}^{(i)}\right)\right)\right)\boldsymbol{\Omega}_k,\\ \mathbf{H}_{q\lambda} &= 2\mathbf{q}^{(i)},\quad \mathbf{H}_{\varepsilon_m\varepsilon_m}=2\,\Pi_k\end{aligned}$$

Step 5: Update the estimate by (17).

Step 6: If the Newton method's termination condition is satisfied, set $k=k+1$ and go to Step 2. Otherwise, set $i=i+1$ and go to Step 4.

As the summation terms $\sum_k \cdot$ can be computed recursively along with the time instant k, we can re-formulate the above batch algorithm in a recursive form in a recursive form as shown in Algorithm 1.

The Newton method's final estimate by Step 6 could be used as an alternative initial value for the next time instant in Step 3, but it requires to carefully check the validness of the final estimate. Otherwise, the convergence the recursive algorithm would be put at stake.

ACKNOWLEDGMENTS

Thanks to Professor Xiaoji Niu, GNSS Research Center in Wuhan University, for recommending the iPhone test.

REFERENCES

[1] *ADI MEMS IMU Products*, accessed on Aug. 2015. [Online]. Available: http://www.analog.com/cn/products/mems/isensor-mems-inertial-measurement-units.html

[2] Y. Wu and W. Shi, "On calibration of three-axis magnetometer," *IEEE Sensors J.*, vol. 15, no. 11, pp. 6424–6431, Nov. 2015.

[3] P. Minotti, S. Brenna, G. Laghi, A. G. Bonfanti, G. Langfelder, and A. L. Lacaita, "A sub-400-nT/$\sqrt{}$Hz, 775-μW, multi-loop MEMS magnetometer with integrated readout electronics," *J. Microelectromech. Syst.*, vol. 24, no. 6, pp. 1938–1950, 2015.

[4] G. L. Frangi, P. Minotti, and G. Langfelder, "Effect of stators geometry on the resonance sensitivity of capacitive MEMS," *Procedia Eng.*, vol. 120, pp. 294–297, 2015.

[5] P. D. Groves, *Principles of GNSS, Inertial, and Multisensor Integrated Navigation Systems*. Boston, MA, USA: Artech House, 2008.

[6] J. Lenz and A. S. Edelstein, "Magnetic sensors and their applications," *IEEE Sensors J.*, vol. 6, no. 3, pp. 631–649, Jun. 2006.

[7] D. Gebre-Egziabher, C. H. Elkaim, J. D. Powell, and B. W. Parkinson, "Calibration of strapdown magnetometers in magnetic field domain," *ASCE J. Aerosp. Eng.*, vol. 19, no. 2, pp. 1–16, 2006.

[8] J. F. Vasconcelos, G. Elkaim, C. Silvestre, P. Oliveira, and B. Cardeira, "Geometric approach to strapdown magnetometer calibration in sensor frame," *IEEE Trans. Aerosp. Electron. Syst.*, vol. 47, no. 2, pp. 1293–1306, Apr. 2011.

[9] J. C. Springmann and J. W. Cutler, "Attitude-independent magnetometer calibration with time-varying bias," *J. Guid., Control, Dyn.*, vol. 35, no. 4, pp. 1080–1088, 2012.

[10] J. Metge, R. Mégret, A. Giremus, Y. Berthoumieu, and T. Décamps, "Calibration of an inertial-magnetic measurement unit without external equipment, in the presence of dynamic magnetic disturbances," *Meas. Sci. Technol.*, vol. 25, no. 12, p. 125106, 2014.

[11] R. Alonso and M. D. Shuster, "TWOSTEP: A fast robust algorithm for attitude-independent magnetometer-bias determination," *J. Astron. Sci.*, vol. 50, no. 4, pp. 433–452, 2002.

[12] R. Alonso and M. D. Shuster, "Complete linear attitude-independent magnetometer calibration," *J. Astron. Sci.*, vol. 50, no. 4, pp. 477–490, 2002.

[13] J. D. Hol, "Sensor fusion and calibration of inertial sensors, vision, ultra-wideband and GPS," Ph.D. dissertation, Dept. Elect. Eng., Linköping Univ., Linköping, Sweden, 2011.

[14] I. Skog and P. Händel, "Calibration of a MEMS inertial measurement unit," presented at the 18th IMEKO World Congr., Metrol. Sustain. Develop., Rio de Janeiro, Brazil, 2006.

[15] H. Zhang, Y. Wu, M. Wu, W. Wu, and X. Hu, "Improved Multi-position Calibration for Inertial Measurement Units," *Meas. Sci. Technol.*, vol. 21, no. 1, pp. 015107-1–015107-11, 2010.

[16] H. Zhang, Y. Wu, M. Wu, X. Hu, and Y. Zha, "A multi-position calibration algorithm for inertial measurement units," presented at the AIAA Guid., Navigat. Control Conf. Exhibit, Honolulu, HI, USA, 2008.

[17] Z. F. Syed, P. Aggarwal, C. Goodall, X. Niu, and N. El-Sheimy, "A new multi-position calibration method for MEMS inertial navigation systems," *Meas. Sci. Technol.*, vol. 18, no. 7, pp. 1897–1907, 2007.

[18] X. Li and Z. Li, "A new calibration method for tri-axial field sensors in strap-down navigation systems," *Meas. Sci. Technol.*, vol. 23, no. 10, p. 105105, Oct. 2012.

[19] M. Kok and T. B. Schön, "Maximum likelihood calibration of a magnetometer using inertial sensors," in *Proc. 19th World Congr. Int. Fed. Automat. Control (IFAC)*, Cape Town, South Africa, 2014, pp. 92–97.

[20] Y. Wu and X. Pan, "Velocity/position integration formula part I: Application to in-flight coarse alignment," *IEEE Trans. Aerosp. Electron. Syst.*, vol. 49, no. 2, pp. 1006–1023, Apr. 2013.

[21] M. Wu, Y. Wu, X. Hu, and D. Hu, "Optimization-based alignment for inertial navigation systems: Theory and algorithm," *Aerosp. Sci. Technol.*, vol. 15, no. 1, pp. 1–17, Jan./Feb. 2011.

[22] J. Nocedal and S. J. Wright, *Numerical Optimization*. New York, NY, USA: Springer, 1999.

[23] Y. Wu, J. Wang, and D. Hu, "A new technique for INS/GNSS attitude and parameter estimation using online optimization," *IEEE Trans. Signal Process.*, vol. 62, no. 10, pp. 2642–2655, May 2014.

Yuanxin Wu (SM'14) received the B.Sc. and Ph.D. degrees in navigation from the Department of Automatic Control, National University of Defense Technology, in 1998 and 2005, respectively.

He is currently a Professor of Navigation and Control with the School of Electronic Information and Electrical Engineering, Shanghai Jiao Tong University. He was with the National University of Defense Technology as a Lecturer from 2006 to 2007 and an Associate Professor from 2008 to 2012. He was a Visiting Post-Doctoral Fellow with the Department of Geomatics Engineering, University of Calgary, Canada, from 2009 to 2010, and was with Central South University as a Professor from 2013 to 2015. His current research interests include inertial-based navigation system, state estimation, and wearable human motion sensing.

He was a recipient of the National Excellent Doctoral Dissertation (2008), the New Century Excellent Talents in University (2010), the Fok Ying Tung Education Fellowship (2012), and the National Science Award for Excellent Young Scientists (2014) in China. He serves as an Associate Editor (2013) of *The Journal of Navigation*, U.K.

Shitu Luo received the B.Sc., M.Sc., and Ph.D. degrees from the National University of Defense Technology in 1998, 2001, and 2005, respectively.

He was with the National University of Defense Technology as a Lecturer from 2006 to 2009 and an Associate Professor from 2010 to 2015. He was a Post-Doctoral Fellow with the Department of Control Science and Engineering, National University of Defense Technology, from 2007 to 2009, and a Visiting Scholar with the Department of Electronic and Electrical Engineering, University of Bath, U.K., in 2014. He is currently the General Manager of Hunan City-Matrix Technology Company, Ltd. His current research interests include indoor navigation technology, underground pipeline survey, and mobile robot.